Veterinary Parasitology 338 (2025) 110556

Contents lists available at ScienceDirect

Veterinary Parasitology

journal homepage: www.elsevier.com/locate/vetpar

The nanoparticulate lipid secretome in the lifecycle of *Oesophagostomum dentatum*: Shedding light on the role in parasitic development

Anna Sophia Feix [a,*], Bärbel Ruttkowski [a], Silvio Kau-Strebinger [b], Anja Joachim [a]

[a] Institute of Parasitology, Department of Biomedical Sciences and Pathobiology, University of Veterinary Medicine Vienna, Vienna, Austria
[b] Institute of Morphology, Department of Biomedical Sciences and Pathobiology, University of Veterinary Medicine Vienna, Vienna, Austria

ARTICLE INFO

Keywords:
Secretome
Extracellular particles
Extracellular vesicles
Parasitic nematodes
Strongylida

ABSTRACT

The parasitic nematode *Oesophagostomum dentatum*, a member of the order Strongylida, commonly infects pigs worldwide. Its secretome includes proteins, bioactive lipids, and extracellular particles shed in changing composition during development. However, the lipid components of the secretome, including their stage-specific variations and functional significance, remain poorly understood. This study aimed to analyze lipid-containing particles shed by larval and adult stages, and to characterize alterations in lipidomic profiles across the developmental stages. Extracellular nanoparticles (NPs) shed by the parasites, representing a less explored component of the secretome, were isolated using ultracentrifugation and subjected to NP tracking. For a detailed lipidomic and metabolomic analysis of the secretome of different *O. dentatum* stages, FTIR and LC-MS/MS were applied. The data were compared across life cycle stages to identify developmental and functional variations. The lipidomic analysis revealed distinct profiles for larval and adult stages, with stage-specific lipid classes and metabolites. Shed particles were found to carry a diverse array of lipids, including phospholipids, sphingolipids, and sterols, as well as fatty acids that may be key for interactions with the host, including immune evasion. Comparative analyses demonstrated developmental shifts in lipid composition, highlighting possible adaptations to larval migration, nodule formation, and adult reproduction. This study provides the first comprehensive lipidomic characterization of *O. dentatum* as a model for gastrointestinal nematodes, unveiling significant stage-specific lipidomic and metabolic adaptations. The detailed analysis of shed nanoparticles as part of the secretome offers new insights into the biology of parasitic nematodes and their interactions with the host environment.

1. Introduction

Parasitic nematodes of the order Strongylida are a diverse group of organisms infecting a wider range of hosts including domestic mammals and humans. *Oesophagostomum dentatum*, the nodule worm of pigs, has previously been implemented as a model for strongylids due to its availability *ex vivo* and *in vitro* (Gasser et al., 2007; Martin et al., 2015; Ondrovics et al., 2016). Previous works described the shedding of proteins, glycans and fatty acids by different stages of this parasite and their potential role in interactions with the host (Joachim et al., 1999a, 1998, 1999b, 2001a, 2001b). Specifically, eicosanoids, bioactive lipids derived from long-chained polyunsaturated fatty acids with a range of functions in mammals and invertebrates (Curtis-Prior, 2004; Stanley, 2014), are produced by *O. denatum* and released in a stage-specific manner (Daugschies and Ruttkowski, 1998). These and other lipids are involved in various processes, including membrane structure, energy storage, and signaling, and have been implicated in parasite development, immune evasion, and host-parasite interactions (Wangchuk et al., 2023).

To expand on the knowledge of lipids shed by *O. dentatum* during its development, we analyzed larvae cultivated for 14 days, corresponding to the early parasitic phase of tissue invasion and nodule formation, including a molt from third stage (L3) to fourth-stage larvae (L4), corresponding to the histotrophic phase of development in nodules in the wall of the large intestines, as well as adult males and females retrieved from the intestinal contents of pigs after experimental infection. We hypothesize that the adaptation to various environments and functions during worm development (i.e. invasion – growth – reproduction) and interactions with the host (i.e. immune evasion), is reflected in the composition of the lipids released into the parasite's direct environment, and that these lipids have the potential to modulate both the parasite's physiology and the host's tissue functions and immune responses.

* Corresponding author. Current address: Department of Animal and Veterinary Sciences, Aarhus University, Tjele, Denmark.
E-mail address: afeix@anivet.au.dk (A.S. Feix).

https://doi.org/10.1016/j.vetpar.2025.110556
Received 28 March 2025; Received in revised form 28 July 2025; Accepted 28 July 2025
Available online 28 July 2025

2. Materials and methods

2.1. Isolation and cultivation of parasite stages

Larvae of *O. dentatum* (L3, L4) were collected and prepared as described previously (Joachim et al., 2001). In brief 100,000 freshly exsheathed L3 were incubated in a 182.5 cm^2 tissue culture flask (VWR, Vienna, Austria) containing 20 mL sterile culture medium [LB broth, Lennox (Roth Lactan, Graz, Austria) with 10 % pig serum, 1 % penicillin-streptomycin-amphotericin B mix, and 0.1 % gentamicin (PAN Biotech GmbH, Aidenbach, Germany)] under 10 % CO_2 at 38.5°C. Medium exchange after sedimentation of the larvae for 8–10 min was carried out twice a week.

At day 14 of culture the medium was removed, and parasites were carefully washed five times with plain RPMI medium (PAN Biotech GmbH) including a change into a fresh culture flask of the same size. The larger L4 (ca. 25 % of the total number of larvae) were separated from the remaining L3 by differential sedimentation (Joachim et al., 2001). After washing and separation L3 and L4 were incubated for another 18 h in 25 mL RPMI under the same conditions as before. Supernatants were then used to collect shed nanoparticles (NPs).

Adult worms were isolated from the contents of large intestines of experimentally infected pigs by agar-gel migration (Slotved et al., 1996). Sexed worms were carefully washed 10 × with prewarmed PBS containing antibiotic/antimycotic mix as above in double concentration, incubated and further incubated in RPMI for NP production as described for the larvae.

2.2. Isolation of metabolites from supernatants

After 18 h of incubation (identified as the time point of maximal NP production with sustained worm viability in a pilot experiment) supernatants were collected and differentially centrifuged at 300×*g* for 5 min and 1200×*g* for 10 min at 4 °C to remove larvae and culture debris. and filtered through a 0.22 μm Rotilabo® filter (Carl Roth, Karlsruhe, Germany). Small NPs were enriched with multiple ultracentrifugation steps using an Optima TLX centrifuge (Beckman Coulter GmbH, Wien, Austria). Initial centrifugation at 124,500×*g* for 1 h at 4 °C with an MLA-50 fixed-angle rotor removed large protein aggregates. This was followed by washing the NP pellet in PBS at 188,700×*g* for 1 h at 4 °C using a TLA-55 rotor and a final collection under the same conditions, then NPs were resuspended in PBS. Particle characterization was performed following MISEV guidelines to the extent feasible (White et al., 2023; Welsh et al., 2024).

2.3. Nanoparticle tracking analysis (NTA)

The quantity, hydrodynamic diameter and size distribution of *O. dentatum* NPs were analyzed using a ZetaView x20 TWIN Laser System 488/640 (Particle Metrix, Inning am Ammersee, Germany), following protocols described by Mehdiani et al. (2015) and Bachurski et al. (2019). The optical setup was optimized using 100 nm polystyrene beads (Applied Microspheres, Mainz, Germany). NPs were diluted 1:1000 in sterile-filtered ddH_2O, and NTA was performed in scatter mode with the 488 nm laser. The following settings were applied: minimum brightness threshold of 30, maximum brightness of 255, minimum area of 10 pixels, maximum area of 1000, fixed temperature of 25 °C, sensitivity of 75, and a shutter speed of 70. Data acquisition and export was performed using the ZetaView software version 8.06.01 SP1 (Particle Metrix). Each analysis was conducted on three biological replicates, with three technical replicates per sample and data curated from 11 positions per run.

2.4. Metabolic fingerprint with Fourier-transform infrared (FTIR) spectroscopy

The metabolic fingerprints of NPs produced by different stages of *O. dentatum* were analyzed using Fourier Transform Infrared (FTIR) spectroscopy. Purified NPs from histotrophic (L3, L4) and adult male and female parasites were examined following protocols outlined by Buchacher et al. (2023) and Wong et al. (2023). Nanoparticles suspensions were prepared and applied to silicon optical microtiter plates (Bruker Optics GmbH, Ettlingen, Germany), then dried at 40°C for 40 min. FTIR spectra were recorded in transmission mode using an HTS-XT microplate adapter connected to a Tensor 27 FTIR spectrometer (Bruker Optics GmbH). The spectral range was set to 4000–500 cm^{-1}, with a resolution of 6 cm^{-1}, averaging 32 interferograms per spectrum, and included background subtraction.

To compare FTIR spectra across parasite stages, data preprocessing involved vector normalization, baseline correction, and second-derivative calculations across the full spectrum using a second-order 9-point Savitzky-Golay algorithm. Spectroscopic ratios of fatty acids (3500–2800 cm^{-1}), proteins (1720–1500 cm^{-1}), and polysaccharides (1200–900 cm^{-1}) were calculated with minor modifications from methods described by Mihály et al. (2017) and Wong et al. (2023). All experiments were conducted in triplicates, with three biological and three technical replicates for each condition.

2.5. Lipid extraction and sample preparation

To analyze the lipid profiles of NPs from different stages of *O. dentatum*, LC-MS/MS was performed using a Vanquish UHPLC system coupled to an Orbitrap Exploris 240 high-resolution mass spectrometer (Thermo Scientific, MA, USA) in both negative and positive electrospray ionization (ESI) modes. Chromatographic separation was achieved on an ACQUITY Premier CSH C18 column (Waters; 2.1 mm × 100 mm, 1.7 μm) with a flow rate of 0.3 mL/min.

The mobile phases consisted of water:acetonitrile (40:60, v/v; phase A) and isopropanol:acetonitrile (90:10, v/v; phase B), modified with 10 mM ammonium acetate + 0.1 % acetic acid for negative mode and 10 mM ammonium formate + 0.1 % formic acid for positive mode. A 23-minute gradient program, including re-equilibration, was used as follows (time in minutes/%B): 0/15, 2.5/30, 3.2/48, 15/82, 17.5/99, 19.5/99, 20/15, and 23/15. The column was maintained at 65 °C, and the autosampler was kept at 4 °C with a 5 μL injection volume.

Mass spectrometry data were acquired in full-scan mode with a resolution of 120,000 over a mass range of 200–1700 *m/z* (scan time: 100 ms) using a radio frequency (RF) lens voltage of 70 %. MS/MS fragmentation spectra were collected via data-dependent acquisition with a resolution of 15,000, scan time of 54 ms, and stepped collision energies of 25 %, 35 %, and 50 %. The cycle time was set to 600 ms. Ion source parameters included a spray voltage of 3250 V (positive mode) or 3000 V (negative mode), sheath gas at 45 psi, auxiliary gas at 15 psi, sweep gas at 0 psi, ion transfer tube temperature at 300 °C, and vaporizer temperature at 275 °C.

Experimental samples were analyzed in a randomized sequence. Quality control (QC) samples were prepared by pooling equal aliquots from each processed sample, with multiple QC injections performed initially to equilibrate the system. A QC sample was injected after every fifth experimental sample to monitor instrument performance. A blank sample was processed to determine and subtract background signals.

Data processing was performed using MS-DIAL. Raw peak intensity data were normalized to the total ion count of all detected analytes (Drotleff and Lammerhofer, 2019). Features were identified based on accurate mass, isotope patterns, MS/MS fragment scoring, retention times, and intra-class elution pattern matching (Drotleff et al., 2020).

2.6. Data analysis

All lipid LC-MS features were manually inspected and reintegrated as necessary to ensure accurate comparison of lipid relative abundances between larvae and adult worm particles of *O. dentatum* (Fahy et al., 2005, 2009). Lipid categories and classes were expressed as a percentage of the total lipidome, while the abundance of individual lipid species was calculated as a percentage of the total abundance within their respective lipid class. Raw spectra underwent baseline correction and smoothing using the Savitzky-Golay method (five smoothing points, third-degree polynomial) before integrating the specified spectral areas. Statistical significance was assessed using ANOVA ($P < 0.05$). Statistical analyses for all figures presenting quantitative data were performed using GraphPad Prism 8.2.1 software. Heat maps of qualitative data representing individual lipidomes were generated using the R-package 3.3.1. Error bars indicate the relative standard deviation of the means, and statistical significance was determined at $P < 0.05$.

3. Results

3.1. Quantitative particulate secretome variations by parasite developmental stages

To gain initial insights into the NPs released by larval as well as male and female adult stages of *O. dentatum*, a detailed study utilizing nanoparticle tracking analysis (NTA) was conducted.

Fourth-stage larvae exhibited the highest particle release during the 18-hour incubation in vesicle-free medium (Fig. 1A).

The particle size distribution analysis revealed that during an 18 h incubation period a minimum concentration of 1×10^8 particles per mL supernatant was achieved across all developmental stages. The size distribution varied among developmental stages. Nanoparticles released by larvae exhibited a range of 50–500 nm, with L3 (Fig. 1B) and L4 (Fig. 1C) larvae predominantly releasing NPs around 100 nm. Nanoparticles released by adult worms were primarily around 150 nm, with a narrower size distribution of 100–300 nm compared to the more

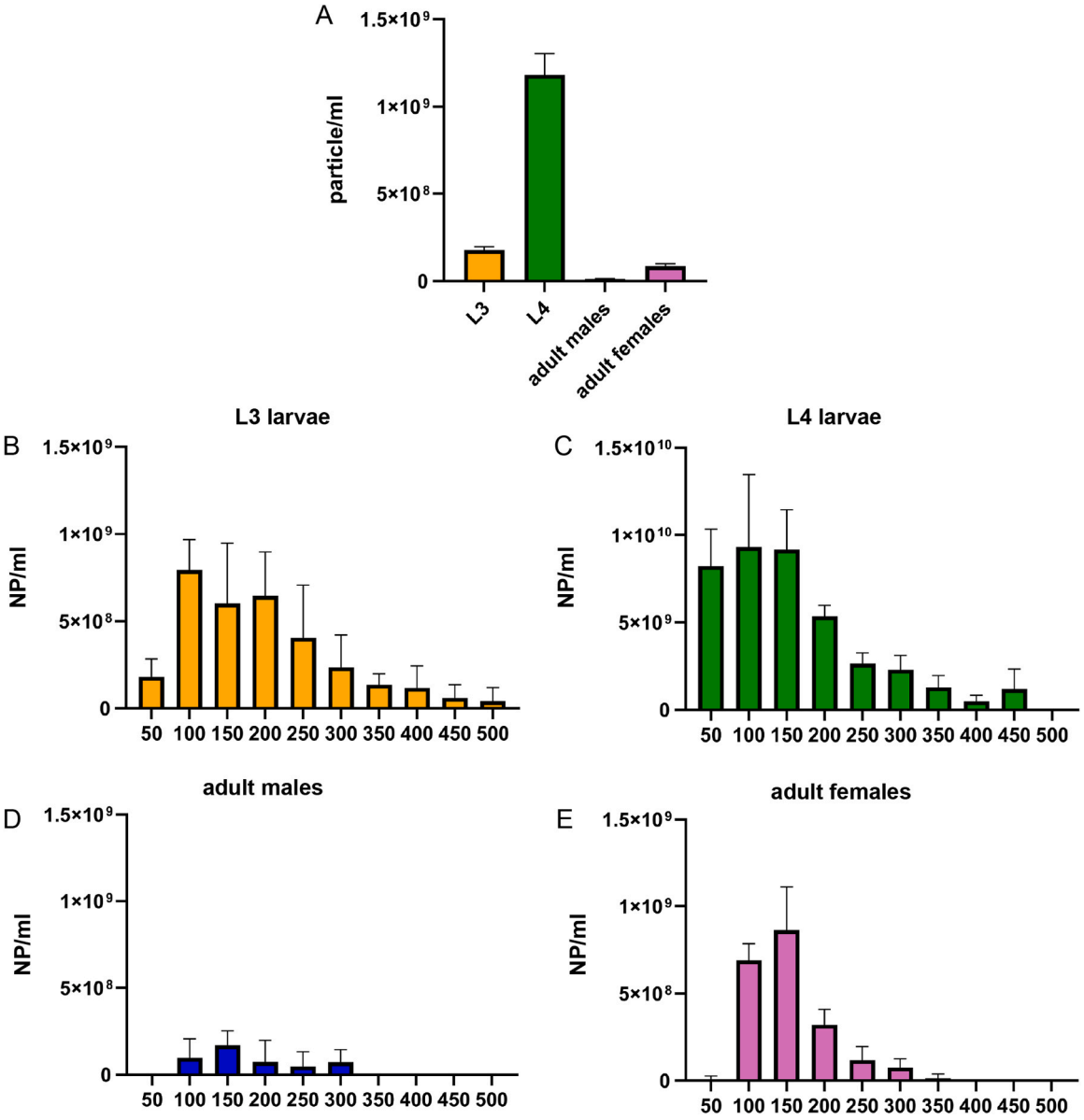

Fig. 1. Size distribution of purified nanoparticles from larvae and adult worms from three independent biological replicates (3 technical measurements each) determined by NTA. A: Particle concentrations released by L3, L4 and male and female adults during a 18 h incubation period; B-D: Size distribution of particles of L3 (B), L4 (C), males (D) and females (E) in the range of 50–500 nm.

heterogeneous distributions observed in larvae. The NP counts were similar among larval stages, while the NP yield from adult worms displayed gender-specific differences. Male adult worms displayed a higher number of larger particles, around 250–300 nm (Fig. 1D) than female adult worms (Fig. 1E), which NPs are mainly sized at around 150 nm.

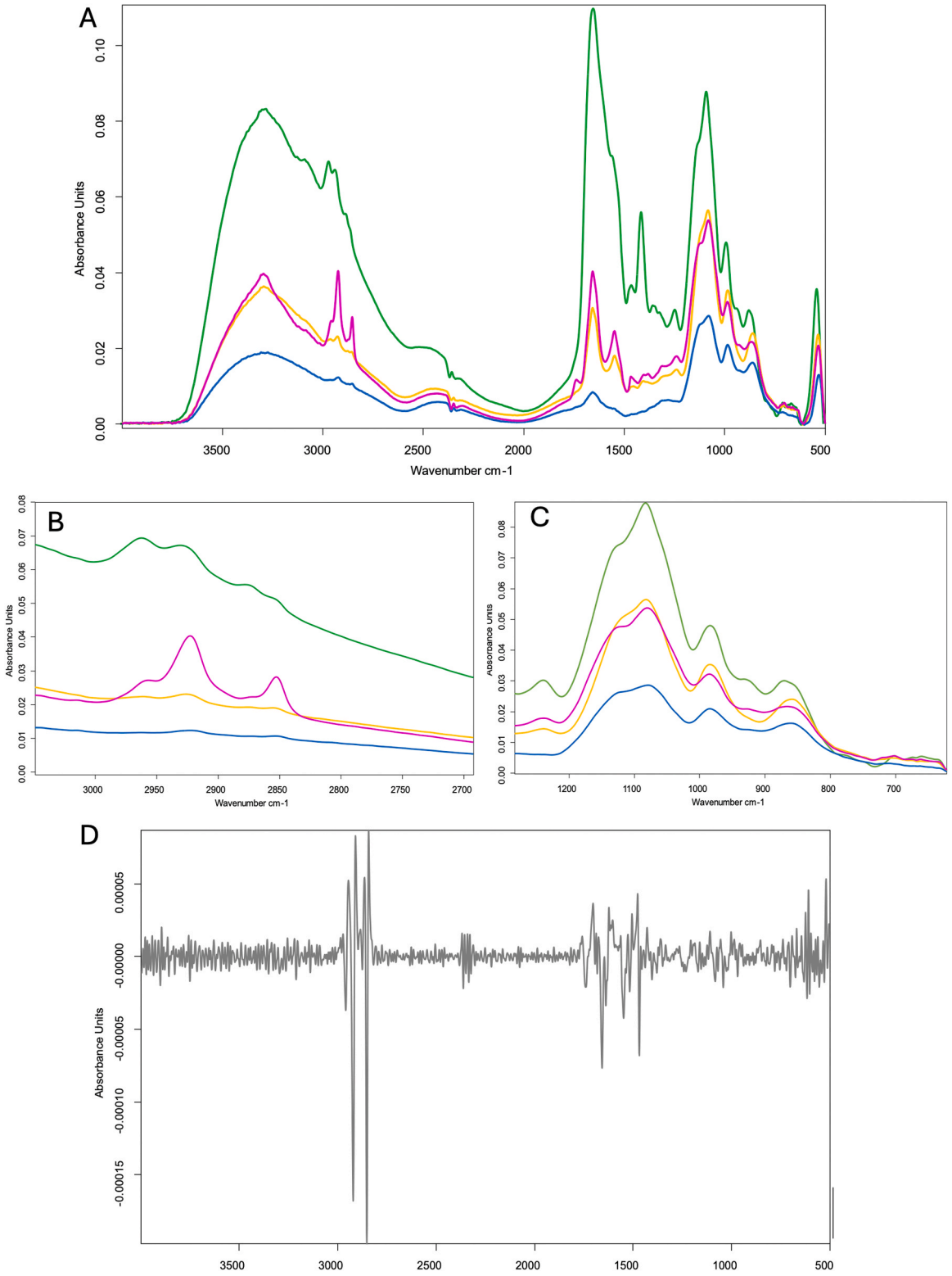

Fig. 2. Fourier transform infrared (FTIR) spectroscopy of nanoparticles shed from different parasite stages (three biological replicates of each stage and 3 technical replicates by biological replicate). A: FTIR of all stages – orange: L3, green: L4, blue: male adult worms, magenta: female adult worms; B: Zoom-in into the region characteristic for phospholipids; C: Zoom-in into the region characteristic for ceramides D: subtraction spectral analysis of the second derivative shows most the most distinct differences between male and female adult worms.

3.2. Metabolic fingerprints of NPs from larvae and adult worm stages

FTIR spectroscopy was employed to further characterize NPs isolated from *O. dentatum* larvae and adult worms, providing detailed metabolic fingerprints of the parasite's secretome. Spectra for nanoparticles from all parasite stages were recorded in the range of 4000–500 cm^{-1} (Fig. 2A). The most prominent differences were observed in the spectral regions corresponding to fatty acids (3500–3000 cm^{-1}), phospholipids and phosphatidylethanolamine (3200–2700 cm^{-1}), and ceramides (1200–700 cm^{-1}). Notably, the highest peaks for phosphatidylethanolamine were identified in L3 larvae and female adult worms, where two distinct peaks were evident (Fig. 2B).

Fatty acids (FAs) starting from C-20 were identified, exhibiting distinct stage- and species-specific patterns. An inverse relationship between FAs and ether-linked lipids in worms during development was evident, with adults showing a higher amount of FAs in comparison to larval stages (Fig. 2A). Ether-linked metabolites were more abundant in larvae and decreased during their development to adults. Within the ceramide spectral region, distinct peaks were observed for all parasite stages, suggesting an increase in ceramide levels from L3 to L4 larvae (Fig. 2C). Additionally, female adult worms exhibited significantly higher ceramide levels compared to males. To further elucidate stage-specific lipid cargos of NPs, subtraction analysis of second-derivative spectra revealed differences in the particle cargo between males and females (Fig. 2D), especially for phospholipids and phosphatidylethanolamine.

3.3. Lipid identification and quantification

The LC-MS/MS lipidomic analysis of lipid extracts from NPs shed by larvae and adults of *O. dentatum* enabled the identification and quantification of 183 lipid species across four lipid superclasses (Fig. 3A): glycerolipids (Fig. 3B), glycerophospholipids (Fig. 3C), sterol lipids (Fig. 3D), and sphingolipids (Fig. 3E). Consistent with available global lipidomic datasets, lipid species from glycerolipids (Fig. 3B) and glycerophospholipids (Fig. 3C) were the most abundant, collectively accounting for approximately 90 % of the identified lipids, followed by sphingolipids (8.74 %), with ceramides and sphingomyelins being the most prevalent species within this class (Fig. 3E).

A total of 46 species of glycerophospholipids were identified, of which 45.65 % were phosphatidylethanolamines, characterized by specific amine groups. *Oesophagostomum dentatum* particles exhibited high levels of unsaturated fatty acids (FAs) and long-chain FAs. Saturated FAs were primarily associated with triacylglycerols (TGs), followed by phosphatidylethanolamines (PEs), whereas ether-linked lipids were predominantly represented by PEs, TGs, and phosphatidylcholines (PCs), with lower contributions from lysophosphatidylethanolamines (LPEs), phosphatidylinositols (PIs), and lysophosphatidylcholines (LPCs).

Ceramides exhibited a stage-specific and gender-specific distribution. In particular, Cer 34:1;O2 and Cer 34:2;O2 showed elevated levels in adult females. Adult males displayed a more uniform and subdued ceramide profile, with minor elevation of Cer 41:1;O2 in specific samples (Fig. 4). Larval stages, while demonstrating some ceramide presence, show a generally lower and more heterogeneous distribution compared to adults, reflecting developmental differences in ceramide

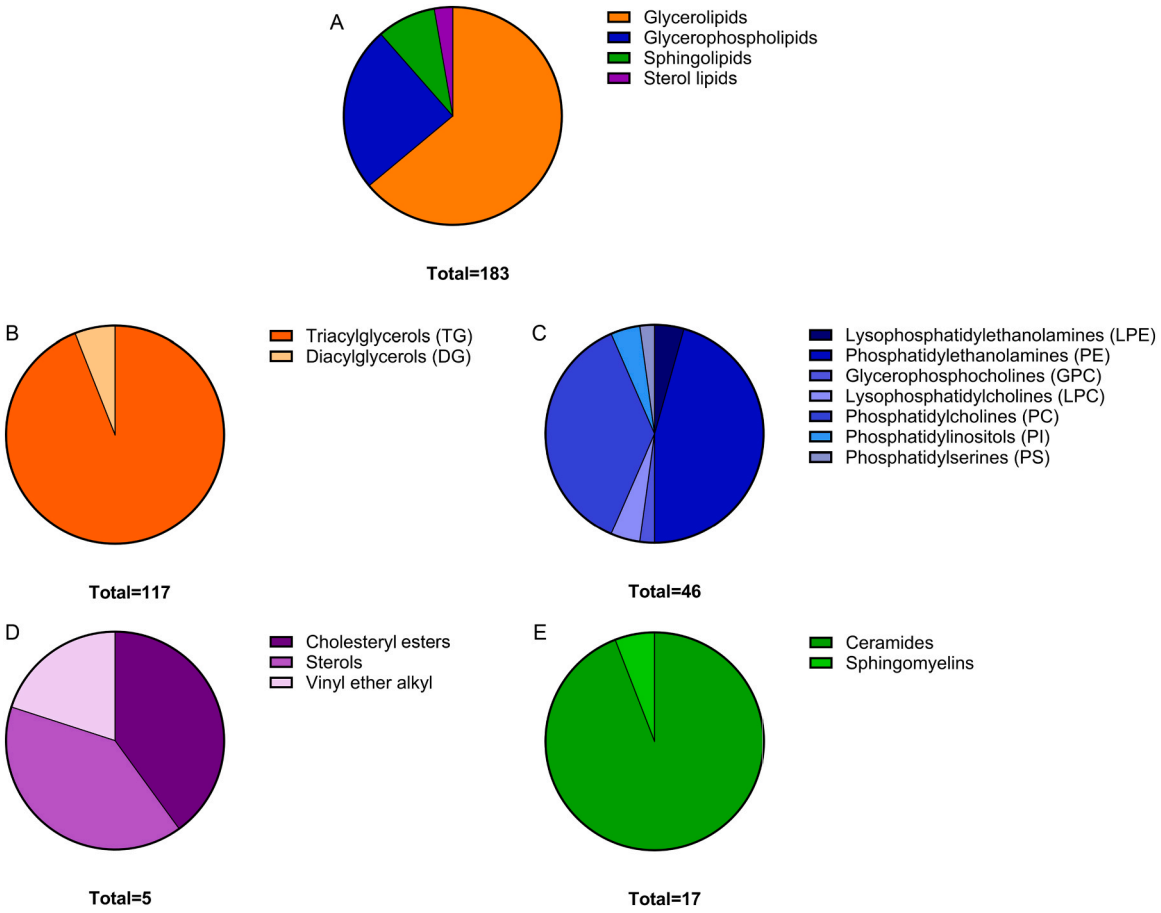

Fig. 3. Quantification of lipid super classes and categories from nanoparticles derived from L3, L4, males and females of *O. dentatum*; A: super classes; B: glycerolipids; C: glycerophospholipids; D: sphingolipids; E: sterol lipids.

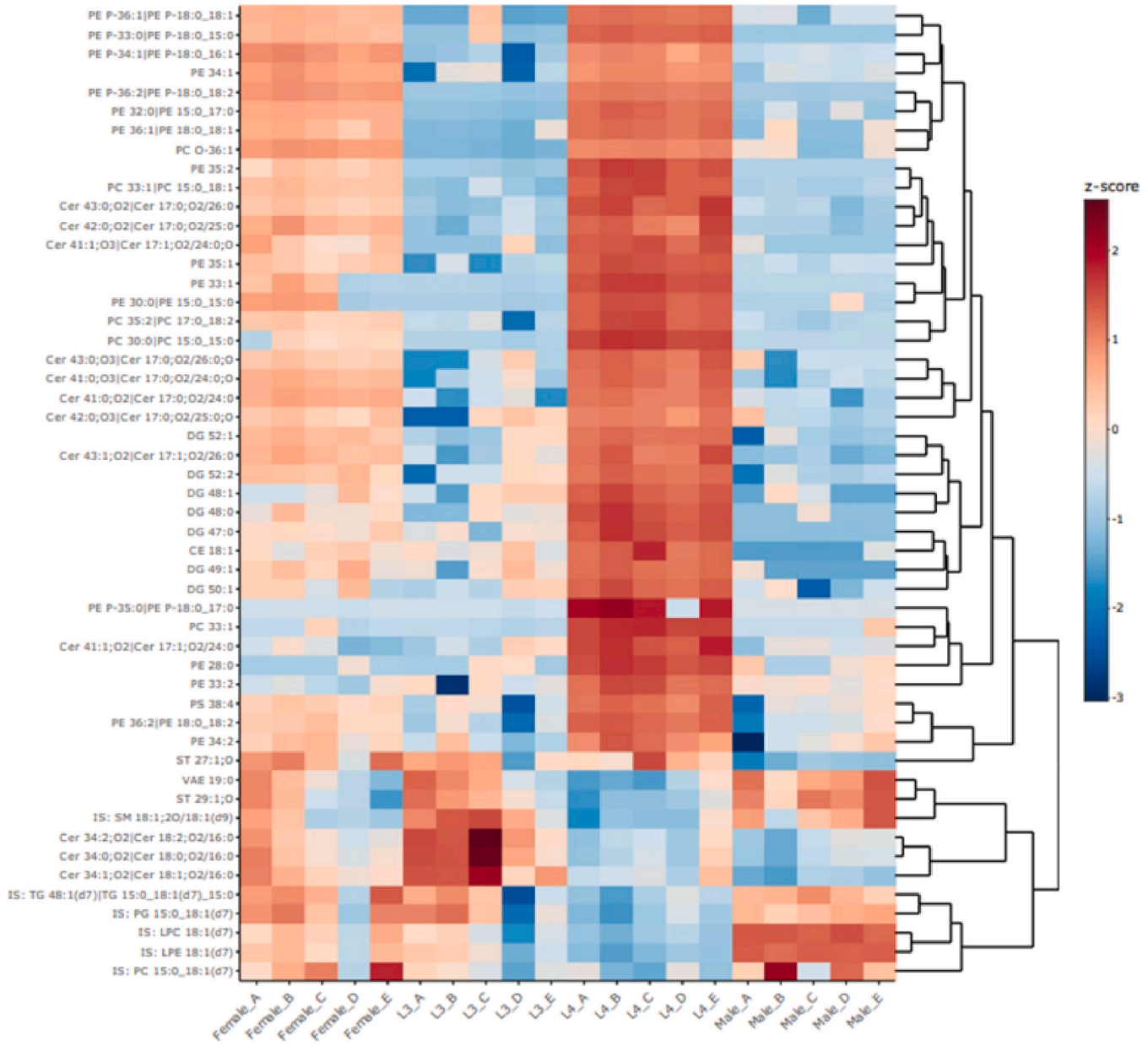

Fig. 4. Unclustered heatmap showing row-wise z-transformed lipid expression across developmental stages of *O. dentatum* sorted according to their expression patterns. Each row represents a different lipid species, higher than average expression in red, average expression white, less than average expression in blue. Each column represents a sample, R1–R5 are five biological replicates each with two technical sub-replicates.

biosynthesis or utilization.

Phosphatidylethanolamines, on the other hand, display distinct abundance patterns compared to ceramides. Phosphatidylethanolamines species such as PE 34:2 and PE 36:2 were markedly elevated in larval stages, particularly in L4, suggesting importance in developmental or metabolic processes during this stage. Adult worms, particularly females, exhibit reduced PE levels overall, with a few exceptions for specific PE species such as PE 35:2 and PE P-36:1. This inverse relationship between ceramides and PEs was particularly evident when comparing L4 larvae and adult females, highlighting a potential metabolic shift between these stages.

For the C20/18:30 lipids, males exhibited the widest and most pronounced log2 FC distribution. Female parasites showed a moderately elevated distribution compared to L3 and L4, which clustered closer to the baseline with smaller variability. A similar pattern was observed in ceramides, where males displayed elevated log2 FC (log2 FC = 0) values with broader variability compared to other stages, which remained relatively constrained around the baseline. Phosphocholides also showed the same trend, with males exhibiting significantly elevated levels compared to females, L3, and L4. These findings highlight potential sex-specific and developmental-stage-related differences in lipid metabolism (Fig. 5).

In the lipid profiles of L3 and L4 (Fig. 6A), the majority of lipid species clustered around log2 fold change, indicating minimal differences between these developmental stages. Exceptions were PE lipids, which exhibit significant changes, with a few species showing downregulation during the transition from L3 to L4. A similar cluster is also shown when comparing the lipids of NPs of adult males and females (Fig. 6B). Comparisons between L3 and male and female adult worms revealed differences between early larval and adult stages (Fig. 6C). PE lipids display variable changes, with a subset significantly upregulated in females compared to L3 (Fig. 6D).

Sterol lipids, glycerolipids, and PE species showed notable upregulation in males compared to L4 (Fig. 6E) but not in the comparison of L4

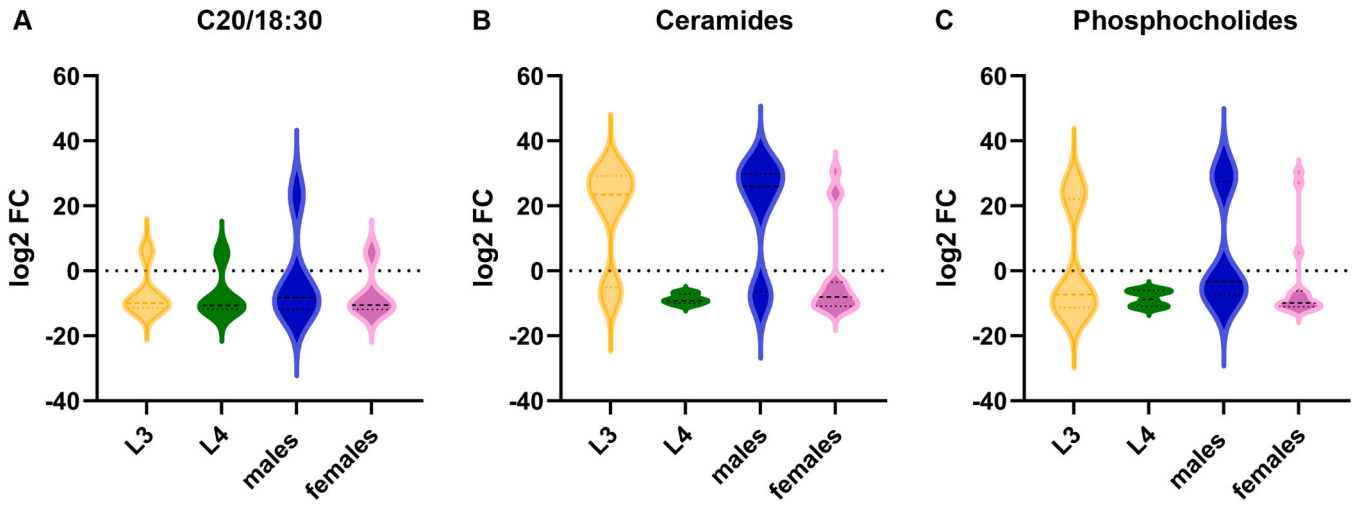

Fig. 5. Violin Plot of C20/18:30 (A), ceramides (B) and phosphocholides (C) of females, males, L3 and L4of *O. dentatum*.

with female worms (Fig. 6F). Ceramides, in contrast, remained relatively stable in the larval stages and exhibited only minimal changes during the transition to adult worms of both sexes. When examining lipids shed via NPs by adult *O. dentatum* worms, a broader distribution became apparent, particularly among phospholipids and sterol lipids. Many PE species show significant upregulation in females compared to males, reflecting distinct metabolic profiles between the sexes (Fig. 6 B).

4. Discussion

Oesophagostomum dentatum is a member of a large order of parasitic nematodes, the Strongylida. Infected pigs excrete eggs with their feces and first-stage larvae develop and hatch. Two molts of the free-living larvae result in infectious, sheathed L3. Upon ingestion, the L3 is exsheathed and the parasitic development is initiated by invasion of the intestinal wall where the larva becomes surrounded by host cells that form the nodule characteristic for this genus. After another molt, the L4 returns to the lumen of the large intestines and continues to grow until after a final molt adult male and female worms are ready to reproduce again (Goodey, 1924). This nematode can be cultivated *in vitro* from egg to pre-adult stage and retrieved from infected pigs as reproductive adults (Joachim et al., 2001). Due to its accessibility and high host adaptation, it has previously been studied as a model to characterize biochemical changes during the development of gastrointestinal parasitic nematodes (Gasser et al., 2007; Martin et al., 2015; Ondrovics et al., 2016; Joachim et al., 1998; 1999a, b, 2000, 2001a, b).

Especially lipids of *O. dentatum* were implicated in its development, reproduction, and survival, although the specific lipid classes and their functions in this species are less explored compared to other nematodes (Barrett, 1968; Medica and Sukhdeo, 1997; Ghosh et al., 2010; Mondal et al., 2016). Our results strongly support the hypothesis that all stages of *O. dentatum* actively produce and secrete NPs of variable sizes into the extracellular milieu during the parasite's development. Heterogenicity among different developmental stages was shown by quantitative analysis via NTA. Larvae stages seemed to shed smaller NPs compared to adult worms; however, all were in the typical size range of small extracellular vesicles (<200 nm) that are mainly released by cells for intercellular communication (Doyle and Wang, 2019). There was a significant difference between the number of particles shed by L3 and L4, with the latter having a 5-fold higher NP release. Furthermore, female adult worms produced significantly more particles than male worms, which might be due to the size differences between the adult stages – as in most other parasitic nematode species, females are considerably longer and thicker than males (Goodey, 1924).

Ceramides play critical roles in parasitic nematodes, particularly in their development, survival, and interactions with the host. As essential components of sphingolipids, ceramides contribute to the structural integrity of cellular membranes and regulate various biological processes (Menuz et al., 2009). This is consistent with high ceramide levels in NPs of all examined stages of *O. dentatum*, as revealed by FTIR and lipidomic analyses. In different studies on nematodes, ceramides exhibit relatively stable patterns, with only a few metabolites showing significant changes (Watts and Ristow, 2017; Wangchuk et al., 2023). This stability likely reflects a conserved role in maintaining cellular structure and signaling during development and sexual differentiation. Ceramides are utilized by parasitic nematodes both for host interactions and as part of their stress response mechanisms, which are vital for their survival (Menuz et al., 2009; Mika et al., 2010). Detailed lipidomic analysis revealed increased ceramide levels in the pre-cultivated L3 larval stage which corresponds to the stage of early histotropic development in the large intestine. This stage requires resilience to survive hostile conditions, including oxidative stress and immune system attacks from the host's environment (more precisely the nodule which comprises a granuloma formed by various host cell types including cells of the reticulo-endothelial system as part of an innate immune response; Schuberth et al., 2000), before transitioning to the L4 stage that leaves the nodule and returns to the proximal large intestines. Male adult worms exhibited higher ceramide levels in comparison to female adult worms. Ceramides are implicated in the modulation of host immune responses and influence nematode excretory-secretory products, which interact with host cells and tissues to suppress immune defenses and establish a parasitic niche. The increased ceramide levels in male worms may contribute to the suppression of host immunity, that might affect not only survival of the worms but also fertility, so that the production of offspring is not hampered by the host (Saccareau et al., 2017).

Fatty acids with a minimum chain length of C-20 were detected in enriched NPs, displaying characteristic stage- and species-specific patterns as observed through FTIR analysis. The L4 stage exhibited the highest peak of fatty acids in FTIR, while detailed lipidomic analysis revealed nearly equal proportions of odd- and even-chained C-20 fatty acids. Previous studies on *O. dentatum* using gas chromatography indicated that particularly histotropic stages show reduced fatty acid diversity (Joachim et al., 2000). These stages are characterized by a predominance of even-chain fatty acids (≥C-16) and a lower abundance of odd-numbered and branched fatty acids. However, in the current study, no significant differences in secreted fatty acids were detected. Previous research also suggested that early developmental stages, such as L3 larvae, contain higher levels of short- and medium-chain fatty acids, which are thought to play a role in energy metabolism and in protecting larvae during their environmental survival phase (Joachim

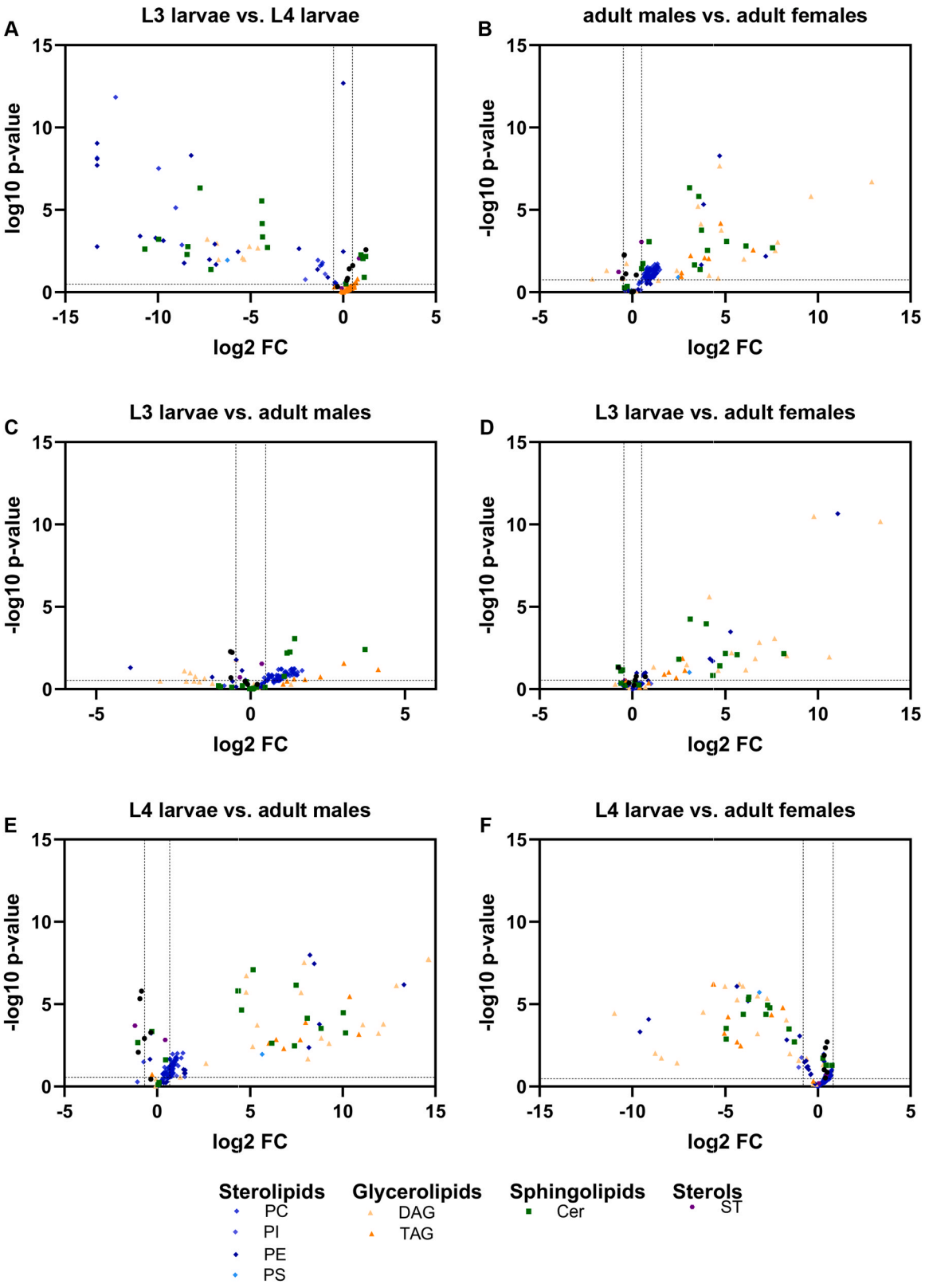

Fig. 6. Direct comparison of lipid species between larvae and adults of *O. dentatum*; Each plot represents the log2 fold change (log2 FC) of lipid species on the x-axis and the negative logarithm of the p-value (-log10 *p*-value) on the y-axis. Lipids with greater significance and larger fold changes appear further from the origin, highlighting significant differences. A: comparison of L3 larvae and L4 larvae, B: comparison of adult males and females, C: comparison of L3 larvae and adult males, D: comparison of L3 larvae and adult females, E: comparison of L4 larvae and adult males, F: comparison of L4 larvae and adult females.

et al., 2000). Furthermore, the inverse relationship between saturated FA and ether-linked lipids is observed across developmental stages, likely due to changes in membrane fluidity, oxidative stress resistance, and energy metabolism. During early stages, such as larval development and host invasion, nematodes increase ether-linked lipids, particularly plasmalogens, to enhance membrane flexibility and protect against oxidative damage from the host's immune system. As they mature into later stages, they accumulate saturated FAs to reinforce membrane rigidity and structural stability. This shift allows nematodes to adapt to environmental stressors, optimize energy efficiency, and regulate lipid biosynthesis based on metabolic demands and host interactions (Mika et al., 2010; Mondal et al., 2016).

Phosphatidylethanolamine (PE), a key phospholipid, is often identified in the secretome of parasitic nematodes and plays important roles in host-parasite interactions (Vanhamme et al., 2020). In some nematodes, such as *Brugia malayi* (Liu and Weller, 1989), *Haemonchus contortus* (Wang et al., 2018) and *Strongylus vulgaris* (Medica and Sukhdeo, 1997), PE has previously been detected as part of the lipid composition of extracellular vesicles. These vesicles are known to mediate communication between parasite and host and are a subfraction of the secreted nanoparticles (Drurey and Maizels, 2021; White et al., 2023). Previous studies showed that early nematode larval stages may release more PE-enriched vesicles as part of the developmental and migration process, while in adult stages, PE may be more prominently involved in immune evasion and nutrient acquisition and therefore might be found at increased concentrations in the secretome of adult worms (Marcilla et al., 2014; Hoffmann et al., 2020; Drurey and Maizels, 2021). This could be also shown in this study. Phosphatidylethanolamine lipids consistently demonstrated significant variability by FTIR and lipidomic analysis, particularly in female worms. This suggests that PE metabolism may play a key role in sex-specific lipid profiles. In contrast, these findings highlight the dynamic regulation of PE lipids, potentially tied to reproductive or developmental processes.

5. Conclusion

This study showed that *O. dentatum* actively produces and secretes nanoparticles of varying number and size into the extracellular environment throughout its developmental stages. These particles also carry lipids, many of which have known roles in lipid metabolism and immunomodulation and therefore permit the assumption that these nanoparticles likely contribute to parasite-host interactions, as shown for other parasitic nematodes. The functional significance of the lipids identified in this study remains an open question, warranting further investigation. The observed differences in nanoparticle lipid composition across L3, L4, and male and female adult worms highlight developmental adaptations to invasion, survival and reproduction of this roundworm and provide an important foundation for future research into parasitic nematodes, employing *O. dentatum* as an accessible model for this group of pathogens.

Author contributions

ASF: data curation and analysis, statistics, manuscript draft; BR: parasite cultivation and collection, manuscript revision; SKS: assistance in data curation, manuscript revision; AJ: financial support, parasite retrieval, principal project supervision, manuscript revision

CRediT authorship contribution statement

Bärbel Ruttkowski: Writing – review & editing, Data curation. **Anna Sophia Feix:** Writing – review & editing, Writing – original draft, Methodology, Formal analysis, Data curation, Conceptualization. **Anja Joachim:** Writing – original draft, Resources, Conceptualization. **Silvio Kau-Strebinger:** Writing – review & editing, Methodology.

Consent for publication

Not applicable.

Ethics approval and consent to participate

All procedures involving animals were approved by the Animal Ethics Committee of the University of Veterinary Medicine Vienna and the national authority according to § 26ff of Animal Experiments Act, Tierversuchsgesetz 2012-TVG 2012 (license number: BMWF-2023–0.088.492; Austrian Federal Ministry of Science, Health and Economy).

Funding

The study was financially supported by the Institute of Parasitology, Vetmeduni Vienna. No external funding was used for this project.

Declaration of Competing Interest

The authors declare no competing interests.

Acknowledgements

We acknowledge the support of the EMBL Metabolomics Core Facility (MCF) in the acquisition and analysis of liquid chromatography-mass spectrometry data. This research was supported using resources of the VetCore Facility of the University of Veterinary Medicine in Vienna.

References

Bachurski, D., Schuldner, M., Nguyen, P.H., Malz, A., Reiners, K.S., Grenzi, P.C., Babatz, F., Schauss, A.C., Hansen, H.P., Hallek, M., Pogge von Strandmann, E., 2019. Extracellular vesicle measurements with nanoparticle tracking analysis - an accuracy and repeatability comparison between NanoSight NS300 and ZetaView. J. Extracell. Vesicles 8 (1), 1596016. https://doi.org/10.1080/20013078.2019.1596016.

Barrett, J., 1968. Lipids of the infective and parasitic stages of some nematodes. Nature 218 (5148), 1267–1268. https://doi.org/10.1038/2181267a0.

Buchacher, T., Digruber, A., Kanzler, M., Del Favero, G., Ehling-Schulz, M., 2023. *Bacillus cereus* extracellular vesicles act as shuttles for biologically active multicomponent enterotoxins. Cell Commun. Signal. 21, 112. https://doi.org/10.1186/s12964-023-01132-1.

Daugschies, A., Ruttkowski, B., 1998. Modulation of migration of *Oesophagostomum dentatum* larvae by inhibitors and products of eicosanoid metabolism. Int. J. Parasitol. 28 (2), 355–362. https://doi.org/10.1016/s0020-7519(97)00153-7.

Doyle, L.M., Wang, M.Z., 2019. Overview of extracellular vesicles, Their origin, composition, purpose, and methods for exosome isolation and analysis. Cells 15 8 (7), 727. https://doi.org/10.3390/cells8070727.

Drotleff, B., Lammerhofer, M., 2019. Guidelines for selection of internal standard-based normalization strategies in untargeted lipidomic profiling by LC-HR-MS/MS. Anal. Chem. 91 (15), 9836–9843. https://doi.org/10.1021/acs.analchem.9b01505.

Drotleff, B., Roth, S.R., Henkel, K., Calderon, C., Schlotterbeck, J., Neukamm, M.A., Lammerhofer, M., 2020. Lipidomic profiling of non-mineralized dental plaque and biofilm by untargeted UHPLC-QTOF-MS/MS and SWATH acquisition. Anal. Bioanal. Chem. 412 (10), 2303–2314. https://doi.org/10.1007/s00216-019-02364-2.

Drurey, C., Maizels, R.M., 2021. Helminth extracellular vesicles: Interactions with the host immune system. Mol. Immunol. 137, 124–133. https://doi.org/10.1016/j.molimm.2021.06.017.

Fahy, E., Subramaniam, S., Brown, H.A., Glass, C.K., Merrill, A.H., Murphy, R.C., Raetz, C.R., Russell, D.W., Seyama, Y., Shaw, W., Shimizu, T., Spener, F., van Meer, G., VanNieuwenhze, M.S., White, S.H., Witztum, J.L., Dennis, E.A., 2005. A comprehensive classification system for lipids. J. Lipid Res. 46 (5), 839–861. https://doi.org/10.1194/jlr.E400004-JLR200.

Fahy, E., Subramaniam, S., Murphy, R.C., Nishijima, M., Raetz, C.R., Shimizu, T., Spener, F., van Meer, G., Wakelam, M.J., Dennis, E.A., 2009. Update of the LIPID MAPS comprehensive classification system for lipids. J. Lipid Res. 50, 9–14. https://doi.org/10.1194/jlr.R800095-JLR200.

Gasser, R.B., Cottee, P., Nisbet, A.J., Ruttkowski, B., Ranganathan, S., Joachim, A., 2007. *Oesophagostomum dentatum*: potential as a model for genomic studies of strongylid nematodes, with biotechnological prospects. Biotechnol. Adv. 25 (3), 281–293. https://doi.org/10.1016/j.biotechadv.2007.01.008.

Ghosh, A., Kar, K., Ghosh, D., Dey, C., Misra, K.K., 2010. Major lipid classes and their fatty acids in a parasitic nematode, *Ascaridia galli*. J. Parasit. Dis. 34 (1), 52–56. https://doi.org/10.1007/s12639-010-0005-4.

Goodey, T., 1924. The Anatomy of *Œsophagostomum dentatum* (Rud.) a nematode parasite of the pig, with observations on the structure and biology of the free-living larvæ. J. Helminthol. 2 (1), 1–14. https://doi.org/10.1017/S0022149X00002960.

Hoffmann, K.F., Hokke, C.H., Loukas, A., Buck, A.H., 2020. Helminth extracellular vesicles: great balls of wonder. Int. J. Parasitol. 50 (9), 621–622. https://doi.org/10.1016/j.ijpara.2020.07.002.

Joachim, A., Ruttkowski, B., Christensen, C.M., Daugschies, A., 1999a. Identification, isolation, and characterization of a species-specific 30-kDa antigen of *Oesophagostomum dentatum*. Parasitol. Res. 85 (4), 307–311. https://doi.org/10.1007/s004360050553.

Joachim, A., Ruttkowski, B., Daugschies, A., 1998. Changes in antigen and glycoprotein patterns during the development of *Oesophagostomum dentatum*. Int. J. Parasitol. 28 (12), 1853–1860. https://doi.org/10.1016/s0020-7519(98)00163-5.

Joachim, A., Ruttkowski, B., Daugschies, A., 1999b. Changing surface antigen and carbohydrate patterns during the development of *Oesophagostomum dentatum*. Parasitology 119, 491–501. https://doi.org/10.1017/s0031182099004965.

Joachim, A., Ruttkowski, B., Daugschies, A., 2001a. Characterisation of stage-specific proteins of *Oesophagostomum dentatum* by preparative isoelectric focusing and lectin blotting. Parasitol. Int. 50 (1), 41–45. https://doi.org/10.1016/s1383-5769(00)00070-2.

Joachim, A., Ruttkowski, B., Daugschies, A., 2001b. *Oesophagostomum dentatum*: expression patterns of enzymes involved in eicosanoid production. Parasitol. Int. 50 (3), 211–215. https://doi.org/10.1016/s1383-5769(01)00077-0.

Joachim, A., Ryll, M., Daugschies, A., 2000. Fatty acid patterns of different stages of *Oesophagostomum dentatum* and *Oesophagostomum quadrispinulatum* as revealed by gas chromatography. Int. J. Parasitol. 30 (7), 819–827. https://doi.org/10.1016/s0020-7519(00)00067-9.

Liu, L.X., Weller, P.F., 1989. *Brugia malayi*: microfilarial polyunsaturated fatty acid composition and synthesis. Exp. Parasitol. 69 (2), 198–203. https://doi.org/10.1016/0014-4894(89)90188-4.

Marcilla, A., Martin-Jaular, L., Trelis, M., de Menezes-Neto, A., Osuna, A., Bernal, D., Fernandez-Becerra, C., Almeida, I.C., Del Portillo, H.A., 2014. Extracellular vesicles in parasitic diseases. J. Extracell. Vesicles 3, 25040. https://doi.org/10.3402/jev.v3.25040.

Martin, R.J., Puttachary, S., Buxton, S.K., Verma, S., Robertson, A.P., 2015. The Conqueror Worm: recent advances with cholinergic anthelmintics and techniques excite research for better therapeutic drugs. J. Helminthol. 89 (4), 387–397. https://doi.org/10.1017/S0022149X1400039X.

Medica, D.L., Sukhdeo, M.V., 1997. Role of lipids in the transmission of the infective stage (L3) of *Strongylus vulgaris* (Nematoda: Strongylida). J. Parasitol. 83 (5), 775–779. https://doi.org/10.2307/3284266.

Mehdiani, A., Maier, A., Pinto, A., Barth, M., Akhyari, P., Lichtenberg, A., 2015. An innovative method for exosome quantification and size measurement. J. Vis. Exp. (95), 50974. https://doi.org/10.3791/50974.

Menuz, V., Howell, K.S., Gentina, S., Epstein, S., Riezman, I., Fornallaz-Mulhauser, M., Hengartner, M.O., Gomez, M., Riezman, H., Martinou, J.C., 2009. Protection of *C. elegans* from anoxia by HYL-2 ceramide synthase. Science 324 (5925), 381–384. https://doi.org/10.1126/science.1168532.

Mihály, J., Deák, R., Szigyártó, I.C., Bóta, A., Beke-Somfai, T., Varga, Z., 2017. Characterization of extracellular vesicles by IR spectroscopy: fast and simple classification based on amide and C\\H stretching vibrations. BBA Biomembr. 1859, 459–466. https://doi.org/10.1016/j.bbamem.2016.12.005.

Mika, A., Golebiowski, M., Szafranek, J., Rokicki, J., Stepnowski, P., 2010. Identification of lipids in the cuticle of the parasitic nematode *Anisakis simplex* and the somatic tissues of the Atlantic cod *Gadus morhua*. Exp. Parasitol. 124 (3), 334–340. https://doi.org/10.1016/j.exppara.2009.11.013.

Mondal, M., Kundu, J.K., Misra, K.K., 2016. Variation in lipid and fatty acid uptake among nematode and cestode parasites and their host, domestic fowl: host-parasite interaction. J. Parasit. Dis. 40 (4), 1494–1518. https://doi.org/10.1007/s12639-015-0718-5.

Ondrovics, M., Gasser, R.B., Joachim, A., 2016. Recent advances in elucidating nematode moulting - prospects of using *Oesophagostomum dentatum* as a model. Adv. Parasitol. 91, 233–264. https://doi.org/10.1016/bs.apar.2015.09.001.

Saccareau, M., Sallé, G., Robert-Granié, C., Duchemin, T., Jacquiet, P., Blanchard, A., Cabaret, J., Moreno, C.R., 2017. Meta-analysis of the parasitic phase traits of *Haemonchus contortus* infection in sheep. Parasit. Vectors 10 (1), 201. https://doi.org/10.1186/s13071-017-2131-7.

Schuberth, H.J., Freigofas, R., Daugschies, A., Leibold, W., 2000. Assessment of antibody-independent cellular cytotoxicity (AICC) of porcine neutrophilic granulocytes by quantitative flow cytometry. Lack of modulation by larval products of *Oesophagostomum dentatum*. J. Vet. Med. B Infect. Dis. Vet. Public Health 47 (8), 607–617. https://doi.org/10.1046/j.1439-0450.2000.00391.x.

Vanhamme, L., Souopgui, J., Ghogomu, S., Ngale Njume, F., 2020. The functional parasitic worm secretome: mapping the place of *Onchocerca volvulus* excretory secretory products. Pathogens 9 (11), 975. https://doi.org/10.3390/pathogens9110975.

Wang, T., Nie, S., Ma, G., Korhonen, P.K., Koehler, A.V., Ang, C.S., Reid, G.E., Williamson, N.A., Gasser, R.B., 2018. The developmental lipidome of *Haemonchus contortus*. Int. J. Parasitol. 48 (12), 887–895. https://doi.org/10.1016/j.ijpara.2018.06.002.

Wangchuk, P., Yeshi, K., Loukas, A., 2023. Metabolomics and lipidomics studies of parasitic helminths: molecular diversity and identification levels achieved by using different characterisation tools. Metabolomics 19 (7), 63 https:// doi: 10.1007/s11306-023-02019-5.

Watts, J.L., Ristow, M., 2017. Lipid and carbohydrate metabolism in *Caenorhabditis elegans*. Genetics 207 (2), 413–446. https://doi.org/10.1534/genetics.117.300106.

White, R., Sotillo, J., Ancarola, M.E., Borup, A., Boysen, A.T., Brindley, P.J., Buzás, E.I., Cavallero, S., Chaiyadet, S., Chalmers, I.W., Cucher, M.A., Dagenais, M., Davis, C.N., Devaney, E., Duque-Correa, M.A., Eichenberger, R.M., Fontenla, S., Gasan, T.A., Hokke, C.H., Kosanovic, M., Kuipers, M.E., Laha, T., Loukas, A., Maizels, R.M., Marcilla, A., Mazanec, H., Morphew, R.M., Neophytou, K., Nguyen, L.T., Nolte-'t Hoen, E., Povelones, M., Robinson, M.W., Rojas, A., Schabussova, I., Smits, H.H., Sungpradit, S., Tritten, L., Whitehead, B., Zakeri, A., Nejsum, P., Buck, A.H., Hoffmann, K.F., 2023. Special considerations for studies of extracellular vesicles from parasitic helminths: a community-led roadmap to increase rigour and reproducibility. J. Extracell. Vesicles 12 (1), e12298. https://doi.org/10.1002/jev2.12298.

Wong, L.W., Mak, S.H., Goh, B.H., Lee, W.L., 2023. The convergence of FTIR and EVs: emergence strategy for non-invasive cancer markers discovery. Diagnostics 13 (1), 22. https://doi.org/10.3390/diagnostics13010022.